03,15

Thermoelectric figure of merit enhancement of solid solutions based on $SrTiO_3$ by mechanical activation

© Yu.S. Orlov[1,2], S.N. Vereshchagin[3], L.A. Solovyov[3], A.A. Borus[2], A.V. Nikitin[4], M.V. Bushinsky[4], S.M. Zharkov[1,2], G.M. Zeer[1], V.S. Bondarev[1,2], Yu.N. Ustyuzhanin[2], M.N. Volochaev,[2], V.A. Dudnikov[2]

[1] Siberian State University,
Krasnoyarsk, Russia
[2] Kirensky Institute of Physics, Federal Research Center KSC SB, Russian Academy of Sciences,
Krasnoyarsk, Russia
[3] Institute of Chemistry and Chemical Technology, Federal Research Center KSC SB RAS,
Russian Academy of Sciences,
Krasnoyarsk, Russia
[4] Scientific and Practical Materials Research Center, National Academy of Sciences of Belarus,
Minsk, Belarus

E-mail: jso.krasn@mail.ru

Received November 2, 2023
Revised November 30, 2023
Accepted December 25, 2023

The influence of high-energy mechanical activation on the thermoelectric properties of polycrystalline $Dy_{0.075}Sr_{0.925}Ti_{1-x}P_xO_3$ ($x = 0,\ 0.01,\ 0.025$) samples has been studied. The synthesized solid solutions have a negative Seebeck coefficient, increasing almost linearly in absolute value with increasing temperature. For all samples, a change in the type of electrical conductivity from semiconductor to metallic is observed. A comparative analysis of the results obtained in the temperature range of 300−800 K showed a significant decrease in electrical resistivity with a slight change in the Seebeck coefficient, increasing the thermoelectric power factor to $12.2\,\mu W/(cm \cdot K^2)$ at $x = 0$. Despite the increase in thermal conductivity measured at temperature 300−673 K, thermoelectric figure of merit ZT of mechanically activated samples at $T = 670$ K is higher than that of those not subjected to mechanical activation. The value of figure of merit $ZT = 0.31$ obtained for $x = 0$ is one of the highest reported in the literature for thermoelectrics based on $SrTiO_3$ at this temperature. Replacing titanium with phosphorus does not improve thermoelectric characteristics. A tendency towards a decrease in electrical resistance and an increase in thermal conductivity as a result of mechanical activation is observed for all studied samples.

Keywords: thermoelectricity, electron microscopy, mechanical activation, solid solutions.

DOI: 10.61011/PSS.2024.03.57936.247

1. Introduction

For a long time the researchers pay attention to applicability of compounds based on strontium titanate (STO) as mixed ion-electron conductor in the modern solid-state ion devices [1], as anode materials for solid-oxide fuel elements [2–6] and oxide thermoelectrical materials of the *n*-type in devices of conversion of thermal energy in air for the average temperatures (up to 800 K) [7–10].

In order to improve efficiency of transformation of thermal energy into electrical one characterized by Q factor $ZT = S^2\sigma T/\kappa$, where S — Seebeck coefficient, σ — electrical conductivity, $\kappa = \kappa_e + \kappa_l$ — thermal conductivity (κ_e and κ_l — electron and lattice thermal conductivity, respectively), T — absolute temperature, approaches are applied, which are related to increasing the power factor $P = S^2\sigma$ and attempts of decreasing the thermal conductivity κ by creating additional scattering phonons via substituting in the positions A or B of the STO perovskite structure with various rare earth elements [11–14], joint doping on the node A and B [15], creating cation and oxygen vacancies [16–18], adding other phases [19], introducing metal inclusions into the sample matrix [20,21] and changing the sample morphology with various synthesis methods and nanostructuring [22,23].

Analysis of the X-ray diffraction data and thermoelectric parameters shows that the best thermoelectric properties of the compounds $R_{1-x}Sr_xTiO_3$ (R — the rare-earth metal) are observed at a doping level x from 0.05 to 0.1. In this case the samples are single-phase ones and have a cubic or tetragonal perovskite structure. The increase in the content of a rare-earth metal results in appearance of the additional phase of the pyrochlore type $R_2Ti_2O_7$ [24,25], thereby resulting in degradation of electrical conductivity and the power factor. The thermoelectrical properties of the rare-earth strontium titanates are substantially affected by process synthesis modes [26]. The study [22] has shown that change of a time of annealing in a reducing atmosphere the air-synthesized $Sr_{0.9}Ln_{0.1}TiO_3$ significantly affects the value of thermoelectrical Q factor. At the same time, there is optimum time of annealing, at which the values ZT and P get the maximum at the minimum thermal conductivity. Substitution of titanium with Nb^{5+} which acts as an electron donor [27], results in increase in the number of the charge

Lattice constants of the main phase and the content of the impurity phases of pyrochlore $Dy_2Ti_2O_7$ (ICDD PDF 04-010-2183) and phosphate $Sr_3D_y(PO_4)_3$ (ICDD PDF 00-029-1299) in the samples $Dy_{0.075}Sr_{0.925}Ti_{1-x}P_xO_3$

$Dy_{0.075}Sr_{0.925}Ti_{1-x}P_xO_3$	a	c	V	Content, mass%	
				$Dy_2Ti_2O_7$	$Sr_3Dy(PO_4)_3$
$x = 0$	5.5119(3)	7.8055(6)	237.14(3)	0.6	–
$x = 0.025$	5.5161(2)	7.8071(2)	237.55(2)	1.2	1.6
$x = 0$ (m/a) [31]	5.5214(2)	7.8128(6)	238.18(3)	9.6	–

carriers and, respectively, increase in electrical conductivity. The similar effect of increased electrical conductivity has been obtained for perovskite $SrCoO_{3-\delta}$ when substituting Co^{3+} with non-metallic phosphorus P^{5+} [28].

The present study has investigated the thermoelectrical properties of $Dy_{0.075}Sr_{0.925}Ti_{1-x}P_xO_3$ ($x = 0$, 0.01, 0.025), examined the method of improving the thermoelectric Q factor by high-energy mechanical activation of the compounds based on strontium titanate and comparatively analyzed the thermoelectrical properties of the mechanically activated and non-mechanically activated samples.

2. Experimental part

The samples $Dy_{0.075}Sr_{0.925}Ti_{1-x}P_xO_3$ ($x = 0$, 0.01, 0.025) were made of a stoichiometric quantity of high-pure oxides TiO_2, Dy_2O_3, strontium carbonate $SrCO_3$ and ammonium dihydrogen phosphate $NH_4H_2PO_4$ as follows. The non-mechanically activated samples were synthesized by a standard ceramic technique: thorough mixing of the initial reagents in an agate mortar using ethanol, annealing of the obtained mixture at $T = 1373$ K, trituration, pressing the annealed mixture into tables with subsequent annealing at the same temperature for 12 h. The cycle of trituration-pressing-annealing was repeated twice. The tablets $T = 1473$ K were finally synthesized for 24 h (DSTPO). Then, a part of the synthesized tablets was again triturated and subjected to high-energy grinding (mechanical activation) in ethanol to nanometer sizes in a planetary micromill (Pulverisettte 7 premium line Fritsch GmbH, Germany) using a grinding jar and tungsten carbide balls of the diameter of 3 mm. After alcohol evaporation, the obtained powder was pressed into the tables, which were annealed at $T = 1473$ K for 24 h (DSTPO-m/a). In order to obtain the temperature dependences of resistivity and the Seebeck coefficient, bars $5 \times 14 \times 1.5$ mm were cut, and thermal conductivity was studied using discs of the diameter of 14 ± 1 mm. Prior to the measurements, all the samples were reduced in a flow of the mixture 5% H_2–He as per the program: heating to 1573 K at the rate of 6°/min, holding at 1573 K for 1 h, cooling in the flow of H_2–He to room temperature.

The surface morphology and degree of crystallinity of the obtained samples were visualized using the scanning election microscope (SEM) JEOL JSM-7001F. The SEM-studies were performed in an electron microscopy laboratory of Collective Use Center of Siberian Federal University.

The temperature dependences of the Seebeck coefficient and resistivity were obtained in an original experimental plant similar to [29] within the temperature range 300–800 K. The relative error of measurement of the Seebeck coefficient was 5%, so was that of resistivity — 2%.

The thermal conductivity of the samples was measured at the temperatures 300–673 K using a thermal conductivity meter IT-λ-400.

3. Results and discussion

The data of X-ray diffraction analysis of the samples $Dy_{0.075}Sr_{0.925}Ti_{1-x}P_xO_3$ (DSPTO-m/a) show that in the sample with $x = 0$ the main phase is tetragonal perovskite with a small amount of pyrochlore $Dy_2Ti_2O_7$ (ICDD PDF 04-010-2183). In addition to pyrochlore, the sample with $x = 0.025$ has also exhibited additional reflexes, which correspond to the mixed phosphate $Sr_3D_y(PO_4)_3$ (ICDD PDF 00-029-1299) (Figure 1, Table). The diffraction pattern of the sample with $x = 0$ is characterized by

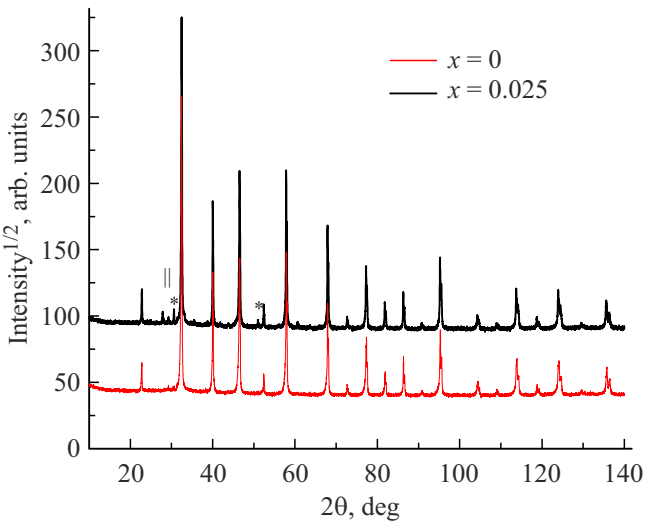

Figure 1. Diffraction patterns of the samples $Dy_{0.075}Sr_{0.925}Ti_{1-x}P_xO_3$ with $x = 0$ (red) and $x = 0.025$ (black). It additionally marks the reflexes of the impurity phases $Dy_2Ti_2O_7$ (*) and $Sr_3D_y(PO_4)_3$ (—).

pronounced asymmetry of the reflexes, which is almost absent in the sample with $x = 0.025$, which can correspond to heterogeneity of the composition. This heterogeneity may results from a process of transition of initially-formed pyrochlore $Dy_2Ti_2O_7$ into perovskite with increasing the quenching time. The reduction of the content of pyrochlore in the sample is accompanied by noticeable reduction of the lattice constants a, c and a volume of the lattice cell V, which well agrees with the large size of the cation Sr^{2+} in comparison with Dy^{3+} [30]. This trend also comprises the published results for the sample $Dy_{0.075}Sr_{0.025}TiO_3$ [31], which contains 9.6 mass% pyrochlore (Table).

Figure 2 shows the micropicture of the nanoscale powder DSTPO-m/a obtained as a result of mechanical activation of the formed bulk perovskite DSTPO. Most of the particles are characterized by no faceting, thereby indicating that these particles are agglomerates that are formed from smaller particles as a result of alcohol evaporation after grinding. At the same time, the image shows that the composition of the evaporated powder also includes bigger clearly-faceted grains with the sizes exceeding 100 nm. As a result of annealing, the particle size increases, wherein the size of the grains of the DSTPO samples is significantly higher than DSTPO-m/a (Figure 3, *a, b*).

The increase in the annealing time of the samples results in stabilization of the DSTPO samples demonstrating reversibility of the resistivity temperature dependences in the heating-cooling modes in the helium atmosphere (the helium purity is 99.999%) unlike the samples investigated in our previous study [31]. At the same time, in the transition semiconductor−metal area, resistivity becomes somewhat less both for DSTPO and the mechanically activated DSTPO-m/a samples, whereas the temperature dependences of the Seebeck coefficient in the studied temperature area become almost linear. The temperature dependences of resistivity $\rho(T)$ of the samples DSTPO and DSTPO-m/a (Figure 4, *a*) demonstrate standard behavior for substituted rare-earth strontium titanates [7,28]. Below a certain transition temperature (TT), there is evidently a semiconductor type of conductivity, i. e. ρ decreases with the temperature increase, while above the TT, the type of conductivity is change to the metal one and resistance linearly increases with the temperature increase. At the same time, resistance of the mechanically activated DSTPO-m/a is significantly lower than for the DSTPO samples, and the TT is shifted into the area of the lower temperatures almost by 150 degrees. We have also observed significant reduction of resistivity as a result of mechanical activation on the compounds $Sr_{1-x}R_xTiO_{3-\delta}$ in the studies [25,31].

It could be expected that addition of phosphorus P^{5+} would contribute to improvement of the thermoelectric parameters. In accordance with a Kreger–Vink record form for $Dy_{0.075}Sr_{0.925}(Ti^{4+}_{1-x-y}Ti^{3+}_yP^{5+}_x)O_3$, substitution of titanium with phosphorus can increase the content of Ti^{3+}, resulting in appearance of additional charge carriers similar to substitution of Ti^{4+} with Nb^{5+} [26,32,33] and, respectively, in improvement of electrical conductivity of

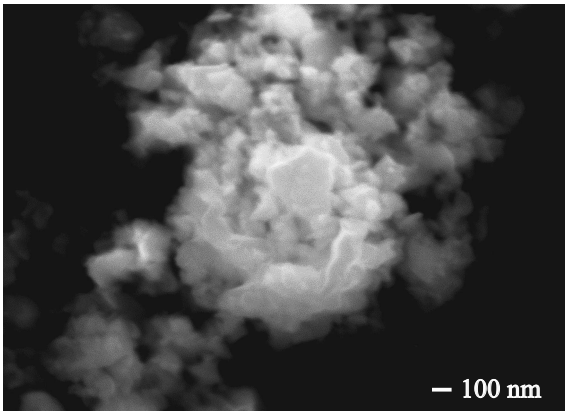

Figure 2. SEM-image of the nanoscale powder $Dy_{0.075}Sr_{0.925}Ti_{1-x}P_xO_3$ after high-energy grinding and evaporation.

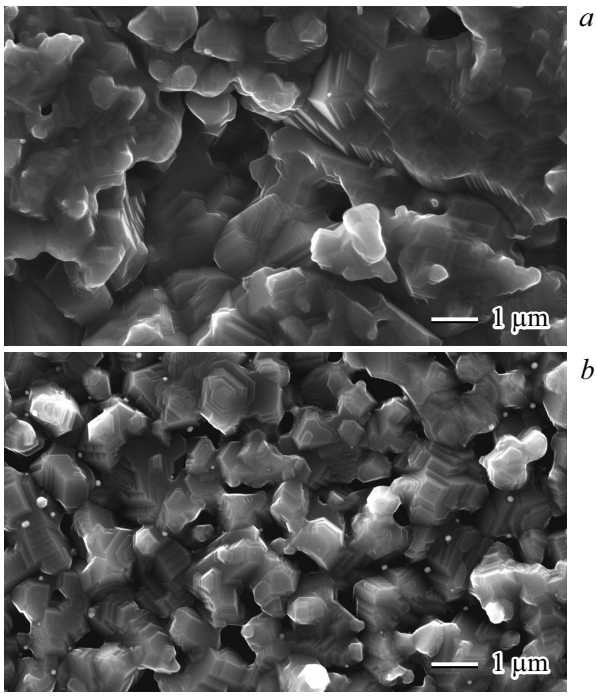

Figure 3. SEM-images of the surface of the samples $Dy_{0.075}Sr_{0.925}Ti_{1-x}P_xO_3$, which are not mechanically activated (DSTPO) (*a*) and mechanically activated (DSTPO-m/a) (*b*).

the samples. Thus, as per the study [28], addition of 5% phosphorus to the composition of the compound $SrCoO_3$ has improved conductivity and stabilized the structure. Besides, the value of lattice thermal conductivity could have been reduced due to additional scattering of phonons on the structure disorder caused by a difference in weights (the molar weight of phosphorus 30.974 g/mol, that of titanium 47.956 g/mol) and in ionic radii (Ti^{3+} — 0.67 Å, P^{5+} — 0.38 Å [30]) for titanium and phosphorus.

However, the temperature dependences of the substituted compounds $Dy_{0.075}Sr_{0.925}Ti_{1-x}P_xO_3$ ($x = 0.01$, 0.025)

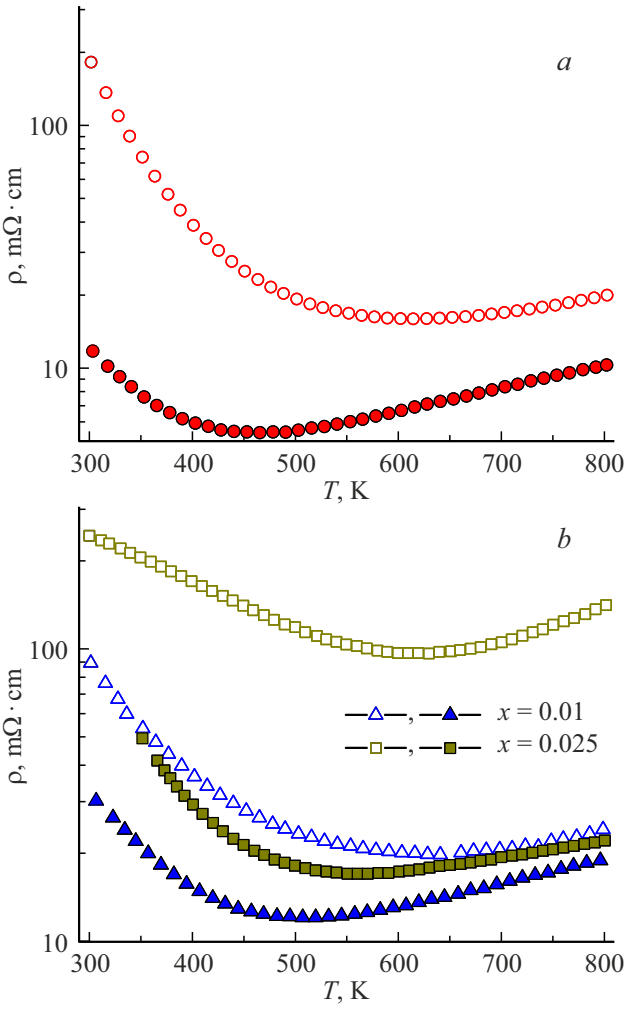

Figure 4. Temperature dependence of resistivity $\rho(T)$ of the samples $Dy_{0.075}Sr_{0.925}TiO_3$ (a) and $Dy_{0.075}Sr_{0.925}Ti_{1-x}P_xO_3$ at $x = 0.01$, 0.025 (b). Hereinafter, empty symbols correspond to the non-mechanically activated samples (DSTPO), so do the solid symbols — to the mechanically activated ones (DSTPO-m/a).

(Figure 4, b) show significant increase in resistivity of the samples with increase in the phosphorus content. The increase in resistance can be related to the impurity phases of phosphate of Dy and pyrochlore, which are present in the sample doped with phosphorus similar to the study [31]. Probably, appearance of the additional centers of scattering due to substitution of titanium with phosphorus becomes a factor resulting in increase in resistance similar to substitution of titanium with thallium, as described in the study [34].

The temperature dependences of the Seebeck coefficient $S(T)$ (Figure 5) for all the samples are almost linear, the absolute values $|S|$ increase with increase in the temperature. The negative values of S indicate an electron n-type of conductivity. Despite the fact that at the room temperature $|S|$ of the DSTPO-m/a samples is somewhat higher that for DSTPO, with increase in the temperature, near 800 K the value of $S(T)$ is almost the same for the activated and non-activate samples at $x = 0$ and $x = 0.01$ (Figure 5, a, b). For $x = 0.025$, vice versa, at the room temperature the values of $S(T)$ are the same, and with increase in the temperature they diverge (Figure 5, b). At the same time, for the activated DSTPO-m/a ($x = 0.025$) the absolute value $|S|$ exceeds that for DSTPO. Thus, mechanical activation somewhat increases the Seebeck coefficient within the temperature range 300–800 K.

The significant reduction of resistivity and weak influence of mechanical activation on behavior of the Seebeck coefficient result in substantial increase in the thermoelectrical power factor (Figure 6). For the compound $Dy_{0.075}Sr_{0.925}TiO_3$ the power factor of the P DSTPO-m/a sample is in 2.5 times higher than for DSTPO (Figure 6, a). With increase in the temperature, there is evidently a trend of plateauing of the dependences $P(T)$, wherein this trend is most pronounced for the mechanically activated samples. Probably, with further increase in the temperature, there will be reduction of P similar to the dependences $P(T)$ of the studies [14,22,27]. The dependences $P(T)$ of Figure 6, b

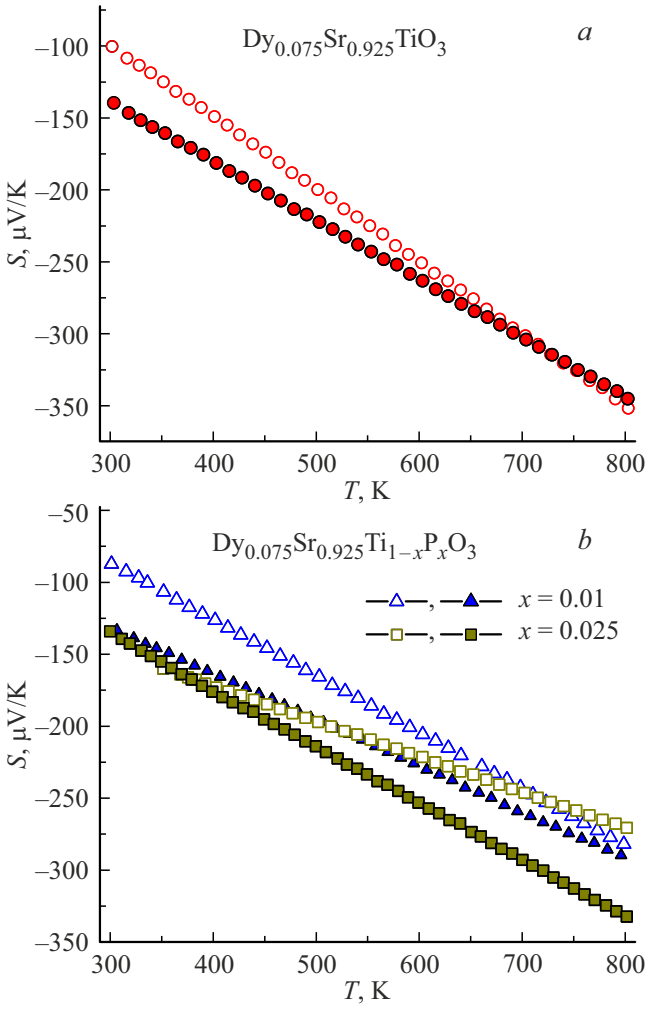

Figure 5. Temperature dependence of the Seebeck coefficient $S(T)$ of the samples $Dy_{0.075}Sr_{0.925}TiO_3$ (a) and $Dy_{0.075}Sr_{0.925}Ti_{1-x}P_xO_3$ at $x = 0.01$, 0.025 (b).

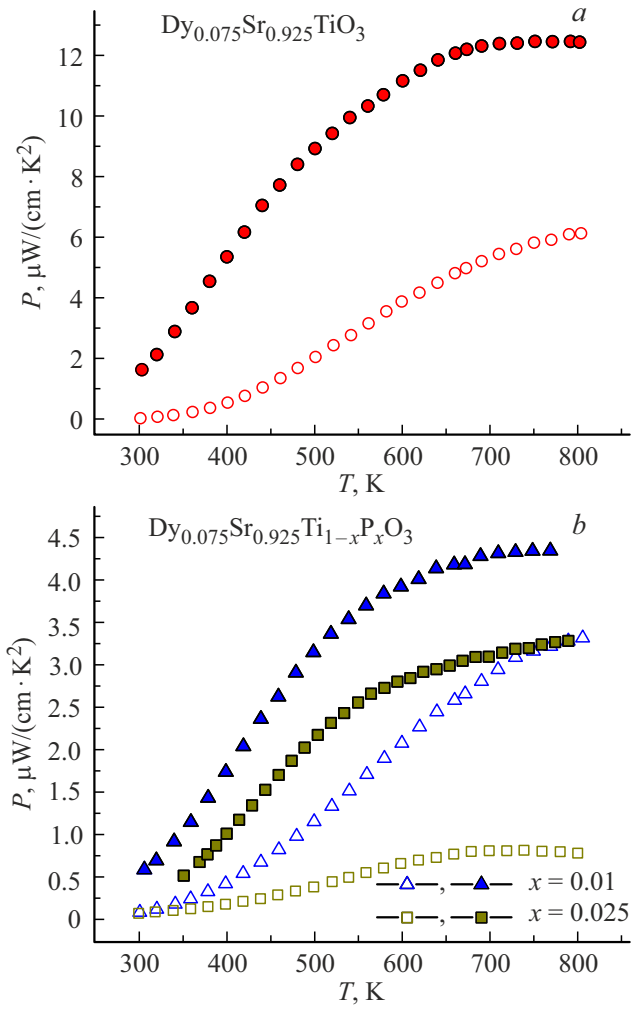

Figure 6. Temperature dependence of the thermoelectrical power factor $P(T)$ of the samples $Dy_{0.075}Sr_{0.925}TiO_3$ (a) and $Dy_{0.075}Sr_{0.925}Ti_{1-x}P_xO_3$ at $x = 0.01,\ 0.025$ (b).

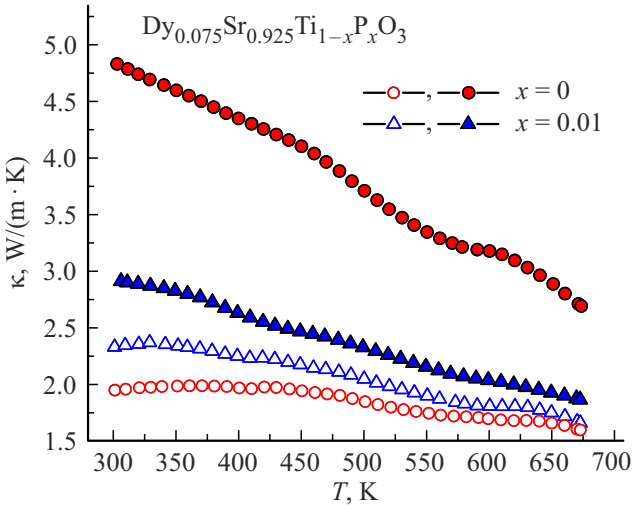

Figure 7. Temperature dependence of thermal conductivity coefficient $\kappa(T)$ for the samples $Dy_{0.075}Sr_{0.925}Ti_{1-x}P_xO_3$ $(x = 0;\ 0.01)$.

demonstrate the reduced power factor with increase in the doping level.

Although, the study [8] has shown reducibility of the thermal conductivity in the nanostructured samples as a result of additional scattering of phonons at the grain boundaries, the measurements performed within the temperature range 300–673 K show that high-energy mechanical activation significantly increases thermal conductivity κ (Figure 7).

The DSTPO thermal conductivity $(x = 0)$ is somewhat less than that of [7] for the compound $Sr_{0.9}Dy_{0.1}TiO_3$, which is most likely related to a different level of substitution with the rare-earth metal. At the same time, the DSTPO-m/a thermal conductivity $(x = 0)$ is numerically close to the data obtained in the study [22].

The increase in thermal conductivity and electrical conductivity due to mechanical activation processing is related to the fact the DSTPO-m/a samples have almost no grain boundary. The mechanically activated samples are a single polycrystalline „sponge“ with well-coalesced grains

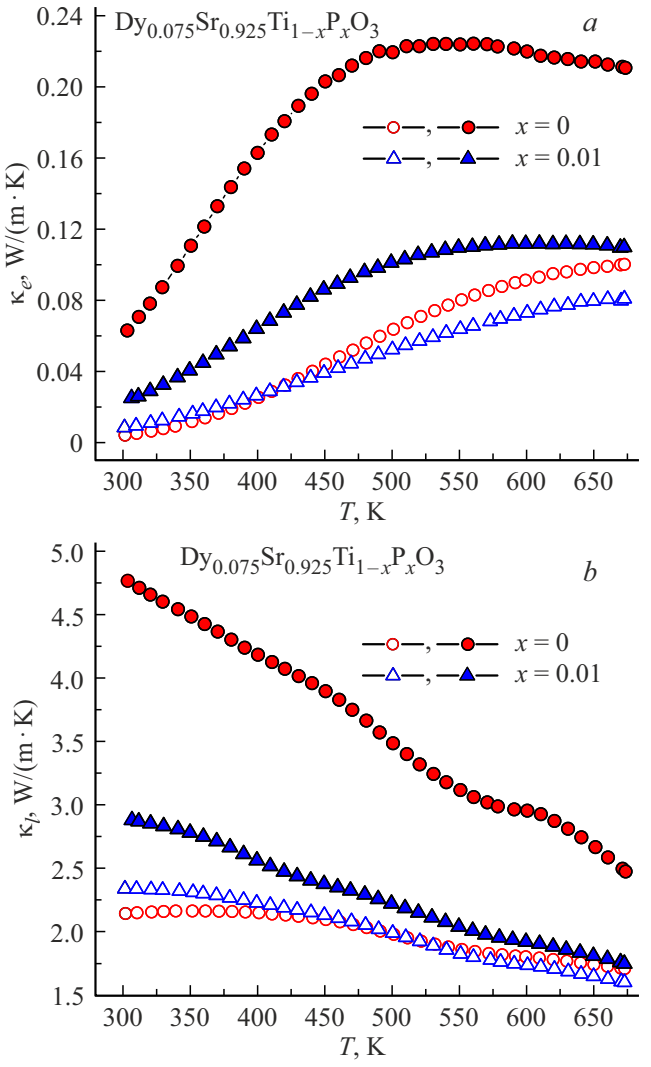

Figure 8. Temperature dependence of the electron κ_e (a) and the lattice κ_l (b) thermal conductivity of the samples $Dy_{0.075}Sr_{0.925}Ti_{1-x}P_xO_3$ $(x = 0;\ 0.01)$.

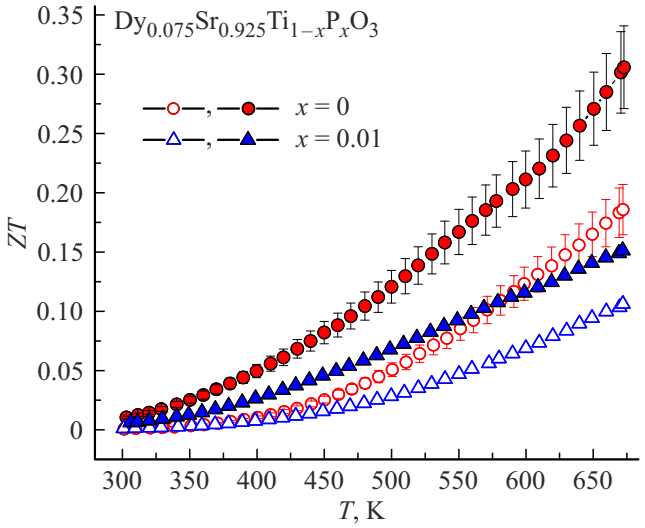

Figure 9. Temperature dependence of the dimensionless thermoelectrical Q factor ZT for the samples $Dy_{0.075}Sr_{0.925}Ti_{1-x}P_xO_3$ ($x = 0$; 0.01). The bars designate an error of the measurements.

(Figure 3, *b*). Despite the fact that the grain size of the DSTPO samples is significantly higher than for DSTPO-m/a, they have clear pronounced boundaries therebetween (they look like cracks, Figure 3, *a*), so the electron and phonon transport is hampered in them.

Figure 8 shows the lattice κ_l and electron κ_e components of thermal conductivity, which are calculated using the Wiedemann–Franz law ($\kappa_e = LT/\rho$, $L = 2.45 \cdot 10^{-8}\,\mathrm{W} \cdot \mathrm{Ohm/K^2}$ — the Lorentz number). The lattice component of thermal conductivity dominates at all the temperatures and decreases with increase in the temperature, wherein the electron component of thermal conductivity is higher for the mechanically activated samples, too.

The thermoelectrical dimensionless Q factor ZT that is calculated from the obtained experimental data is shown on Figure 9. Although, thermal conductivity of the DSTPO-m/a is higher than for DSTPO, the high Q factor P allows obtaining quite high values of ZT at $T = 673\,\mathrm{K}$ for them.

Based on the literature data, the best values of ZT near 673 K for the samples based on the rare-earth strontium titanates are about 0.24 [9,13], 0.33 [19], 0.35 (at 500 K) [35]. In our case, at $T = 673\,\mathrm{K}$ $ZT = 0.31$ is obtained, which is one of the highest values of thermoelectrical Q factor, which are reported for any thermoelectric based on $SrTiO_3$ at this temperature.

4. Conclusion

The present study has synthesized a series of the samples $Dy_{0.075}Sr_{0.925}Ti_{1-x}P_xO_3$ ($x = 0$, 0.01, 0.025) both by the standard ceramic technique and from the nanoscale powder obtained by high-energy mechanical activation. The obtained temperature dependences of the thermoelectric parameters within the temperature range 300–800 K have been comparatively analyzed to show substantial reduction of resistivity with insignificant change of the Seebeck coefficient and increase in thermal conductivity of the mechanically activated samples. The thermoelectrical Q factor ZT of the mechanically activated samples at $T = 670\,\mathrm{K}$ is almost in two times higher than those without mechanical activation. The value of Q factor $ZT = 0.31$ obtained for $x = 0$ is one of the highest ones reported in the literature for the thermoelectrics based on $SrTiO_3$ at this temperature. And it still has a tendency to grow with increase in the temperature, so mechanical activation can be considered as a method of increasing Q factor of this class of the materials. It should be noted that the temperatures of synthesis (1473 K) and reduction of the samples (1573 K) are significantly lower than those usually given in the literature (1673–1773 K).

The substitution of titanium with phosphorus does not improve the thermoelectric characteristics, but it confirms a trend of reduction of electric resistance and increase in thermal conductivity due to mechanical activation, which is observed for all the studied samples.

The literature data have been analyzed to show that in order to achieve the maximum values of thermoelectric Q factor for the compounds based on strontium titanates, it is important to select the substituting rare earth element [36], find an optimum time of sample annealing in the reduction atmosphere [22], and to determine an actual size of the initial nanoparticles [37], the methods of pressing [38] and annealing [39].

Together with the results of this study, accurate selection of the optimum conditions at all stages of sample preparation will most likely allow additionally improving the Q factor value of these promising thermoelectric materials.

Funding

The study was supported by the Russian Foundation for Basic Research (grant No. 20-52-04008 Bel_mol_a). The XPA studies are performed within the scope of the project 0287-2021-00-13.

Conflict of interest

The authors declare that they have no conflict of interest.

References

[1] X. Li, H. Zhao, D. Luo, K. Huang. Mater. Lett. **65**, 2624 (2011).
[2] Q. Ma, F. Tietz, D. Stover. Solid State Ionics **192**, 535 (2011).
[3] C. Savaniu, J. Irvine. Solid State Ionics **192**, 491 (2011).
[4] D. Fagg, V. Kharton, A. Kovalevsky, A. Viskup, E. Naumovich, J. Frade. J. Eur. Ceram. Society **21**, 1831 (2001).
[5] O.A. Marina, N.L. Canfield, J.W. Stevenson. Solid State Ionics **149**, 21 (2002).
[6] S. Singh, P. Singh, M. Viviani, S. Presto. Int. J. Hydrogen Energy **43**, 19242 (2018).

[7] H. Muta, K. Kurosaki, S. Yamanaka. J. Alloys Comp. **350**, 292 (2003).
[8] K. Koumoto, Y. Wang, R. Zhang, A. Kosuga, R. Funahashi. Ann. Rev. Mater. Res. **40**, 363 (2010).
[9] A.V. Kovalevsky, A.A. Yaremchenko, S. Populoh, A. Weidenkaff, J.R. Frade. J. Appl. Phys. **113**, 053704 (2013).
[10] D. Srivastava, C. Norman, F. Azough, M.C. Schrhfer, E. Guilmeau, R. Freer. J. Alloys Comp. **731**, 723 (2018).
[11] C.-S. Park, M.-H. Hong, H.H. Cho, H.-H. Park. J. Eur. Ceram. Soc. **38**, 125 (2018).
[12] T. Okuda, K. Nakanishi, S. Miyasaka, Y. Tokura. Phys. Rev. B **63**, 113104 (2001).
[13] J. Liu, C. Wang, W. Su, H. Wang, J. Li, J. Zhang, L. Mei. J. Alloys Comp. **492**, L54 (2010).
[14] H. Wang, C. Wang, W. Su, J. Liu, Y. Zhao, H. Peng, J. Zhang, M. Zhao, J. Li, N. Yin, L. Mei. Mater. Res. Bull. **45**, 809 (2010).
[15] X. Li, H. Zhao, D. Luo, K. Huang. Mater. Lett. **65**, 2624 (2011).
[16] Z. Lu, H. Zhang, W. Lei, D.C. Sinclair, I.M. Reaney. Chem. Mater. **28**, 925 (2016).
[17] C. Chen, T. Zhang, R. Donelson, T.T. Tan, S. Li. J. Alloys Comp. **629**, 49 (2015).
[18] J. Han, Q. Sun, Y. Song. J. Alloys Comp. **705**, 22 (2017).
[19] M. Qin, Z. Lou, P. Zhang, Z. Shi, J. Xu, Y. Chen, F. Gao. ACS Appl. Mater. Interfaces **12**, 53899 (2020).
[20] D. Srivastava, C. Norman, F. Azough, M.C. Schafer, E. Guilmeau, R. Freer. J.Alloys Comp. **731**, 723 (2018).
[21] M. Qin, F. Gao, G. Dong, J. Xu, M. Fu, Y. Wang, M. Reece, H. Yan. J. Alloys Comp. **762**, 80 (2018).
[22] F. Azough, A. Gholinia, D.T. Alvarez-ruiz, E. Duran, D.M. Kepaptsoglou, A. Eggeman, Q.M. Ramasse, R. Freer. ACS Appl. Mater. Interfaces **11**, 32833 (2019).
[23] J. Wang, B.-Y. Zhang, H.-J. Kang, Y. Li, X. Yaer, J.-F. Li, Q. Tan, S. Zhang, G.-H. Fan, C.-Y. Liu, L. Miao, D. Nan, T.-M. Wang, L.-D. Zhao. Nano Energy **35**, 387 (2017).
[24] J. Liu, C.L. Wang, Y. Li, W.B. Su, Y.H. Zhu, J.C. Li, L.M. Mei. J. Appl. Phys. **114**, 223714 (2013).
[25] Yu. Orlov, S. Vereshchagin, S. Novikov, A. Burkov, A. Borus, M. Sitnikov, L. Solovyov, M. Volochaev, V. Dudnikov. Ceram. Int. **47**, 28992 (2021).
[26] K. Koumoto, Y. Wang, R. Zhang, A. Kosuga, R. Funahashi. Annu. Rev. Mater. Res. **40**, 363 (2010).
[27] K. H. Lee, S. W. Kim, H. Ohta, K. Koumoto. J. Appl. Phys. **100**, 063717 (2006).
[28] Y. Zhu, W. Zhou, J. Sunarso, Y. Zhong, Z. Shao. Adv. Func. Mater. **26**, 5862 (2016).
[29] A. Burkov, A. Fedotov, A. Kasyanov, R. Panteleev, T. Nakama. Sci. Tech. J. Inform. Technol. Mech. Opt. **15**, 173 (2015).
[30] R.D. Shannon. Acta Crystallographica A **32**, 751 (1976).
[31] Yu.S. Orlov, S. Vereshchagin, L. Solovyov, A. Borus, M. Volochaev, A. Nikitin, M. Bushinsky, R. Lanovsky, G. Rymski, V. Dudnikov. J. Taiwan Institute Chem. Eng. **138**, 104449 (2022).
[32] H. Ohta. Mater. Today **10**, 44 (2007).
[33] S. Ohta, T. Nomura, H. Ohta, M. Hirano, H. Hosono, K. Koumoto. Appl. Phys. Lett. **87**, 092108 (2005).
[34] H. Wang, C. Wang, W. Su, J. Liu, H. Peng, Y. Sun, J. Zhang, M. Zhao, J. Li, N. Yin, L. Mei. Ceram. Int. **37**, 2609 (2011).
[35] A.M. Dehkordi, S. Bhattacharya, J. He, H.N. Alshareef, T.M. Tritt. Appl. Phys. Lett. **104**, 193902 (2014).
[36] A.V. Kovalevsky, A.A. Yaremchenko, S. Populoh, P. Thiel, D.P. Fagg, A. Weidenkaff, J.R. Frade. Phys. Chem. Chem. Phys. **16**, 26946 (2014).
[37] M. T. Buscaglia, F. Maglia, U. Anselmi-Tamburini, D. Marre, I. Pallecchi, A. Ianculescu, G. Canu, M. Viviani, M. Fabrizio, V. Buscaglia. J. Eur. Ceram. Society **34**, 307 (2014).
[38] Y. Wang, H.J. Fan. Scripta Materialia **65**, 190 (2011).
[39] P. Roy, V. Pal, T. Maiti. Ceram. Int. **43**, 12809 (2017).

Translated by M.Shevelev